Fuel 360 (2024) 130589

Contents lists available at ScienceDirect

Fuel

journal homepage: www.elsevier.com/locate/fuel

Full length article

Estimation and testing of single-step oxidation reactions for hydrogen and methane in low-oxygen, elevated pressure conditions

Jordan A.C. Kildare [a,*], Michael J. Evans [b], Zhao Tian [a], Paul R. Medwell [a]

[a] School of Electrical and Mechanical Engineering, The University of Adelaide, Adelaide, 5005, Australia
[b] UniSA STEM The University of South Australia, Mawson Lakes, 5095, Australia

ARTICLE INFO

Keywords:
Autoignition
Mild combustion
Combustion theory
Hydrogen combustion
Pressurised combustion

ABSTRACT

Advanced combustion concepts, such as moderate or intense low-oxygen dilution (MILD) combustion, offer a reduction in NO_x emissions and increased thermal efficiency. MILD is characterised by low-oxygen, high-temperature conditions, where finite-rate chemistry effects are significant. Modelling this regime using reduced or single-step chemistry remains a challenge in part due to the finite-rate chemistry. This work proposes a generalised method for assigning Arrhenius coefficients of a single-step reaction using the outputs of a detailed mechanism. Assigning the typical chemical conservation equation to a progress variable, activation energy and pre-exponential factor for an Arrhenius kinetics global reaction are determined for hydrogen and methane across a number of conditions, with the proposed method extended to *n*-heptane as well. The temperature exponent in the modified Arrhenius equation is determined by minimising the ignition delay error between detailed and single-step simulations. Functional forms of each coefficient are calculated from a multivariate regression, dependent on initial temperature, pressure, and oxidant mole fraction. The predicted mechanisms are compared against the detailed kinetics in closed homogeneous batch reactors, with comparisons for hydrogen extended to both laminar opposed flow diffusion flames, and computational fluid dynamics (CFD) simulations. Ignition delay and equilibrium temperature are both well predicted for all three fuels in the batch reactors. Notably, the negative temperature coefficient behaviour of *n*-heptane is successfully recreated with the single-step mechanism. Temperature and heat release of hydrogen flames are well captured in both opposed flow laminar flames, and in turbulent CFD simulations. The computational time was also significantly reduced through the single-step mechanisms, resulting in ~100 times reduction in compute time for CFD simulations. The function form of the Arrhenius coefficients shows promise for extension outside of the ranges and fuels analysed herein, and presents interesting phenomena for exploring how initial reactant temperature and pressure influence the effective activation energy of an oxidation process.

1. Introduction

Despite the shift towards renewable energy sources such as hydro, solar, and wind power, combustion remains a cornerstone of modern society. Under all forecast scenarios, this will remain the case for decades to come [1], and so improving fundamental understanding of advanced combustion concepts remains an important focus for research [2]. Moderate or intense low-oxygen dilution (MILD) combustion is an advanced combustion technique which reduces the production of thermal NO_x by reducing the peak temperatures in a combusting system, with example applications in industrial furnaces at atmospheric pressure and sequential gas turbines at pressures of up to 40 atm [3–5]. It is typically achieved by the mixing of hot products of lean combustion with fresh reactants, raising the equivalent unburnt stoichiometric reactant temperature to above fuel autoignition and providing a low-oxygen (3%–12% by vol.) environment for further reactions [6–8]. These conditions result in a semi-homogeneous mixture that reacts volumetrically, increasing average temperature, but reducing the peak temperatures that cause thermal NO_x formation [4,9,10].

The process of achieving MILD combustion, either through exhaust gas recirculation (EGR), or through sequential combustion staging, results in an increase in thermal efficiency [11]. The higher initial reactant temperature increases the proportion of fuel consumed, improving fuel efficiency, and raising the average temperature of the products [4,12,13]. However, the peak temperatures are reduced as the reaction zone tends towards uniformity, resulting in a reduction in thermal NO_x production [14]. In addition to the increased fuel efficiency,

* Corresponding author.
E-mail address: jordan.kildare@adelaide.edu.au (J.A.C. Kildare).

https://doi.org/10.1016/j.fuel.2023.130589
Received 10 July 2023; Received in revised form 25 October 2023; Accepted 5 December 2023
Available online 9 December 2023

useful radiative heat flux tends to increase in MILD combustion as well, contributing to higher thermal efficiency of this regime [15,16]. Despite the increase in radiative heat flux, MILD has the propensity to suppress the production of soot, a highly radiative combustion product, thus reducing heat transfer [17,18]. The high initial temperatures of MILD combustion also provide another advantage, which is fuel flexibility [19–22]. Experiments involving hydrogen [23,24], methane [14,25], ethanol [20,26], ethylene [27], *n*-heptane [5,19,28], pulverised coal [29–31], biomass [32,33], and fuel oils [10,34,35] have achieved conditions that can be classified as MILD. The oxidant also has flexibility, provided that a low-oxygen environment is still achieved, with O_2/N_2 [36], O_2/H_2O [36], O_2/CO_2 [37], $O_2/N_2/CO_2$ [38], and $O_2/N_2/H_2O/CO_2$ [39] oxidants all achieving MILD combustion. As such, classification of regimes of MILD combustion becomes an important feature in advancing knowledge of stable, robust combustion concepts [40].

Classification of MILD combustion helps to characterise the conditions under which this regime occurs, the fuels for which it is viable, and the limits of applications outside of research [40,41]. The seminal definition for a perfectly stirred reactor (PSR) states that MILD combustion occurs when the temperature of the reactants is above the fuel autoignition temperature, and the temperature rise from combustion is less than the autoignition temperature [4]. This is summarised mathematically as $T_{ai} < T_{in}$, and $\Delta T < T_{ai}$, where subscripts *ai* and *in* refer to autoignition, and initial, respectively [4]. Despite recent extension to nonadiabatic conditions [42], and the capability of providing clear limits of temperature, the foundation of this definition lies in idealised batch reactors, and as such is not readily applicable for turbulent non-premixed flames [43]. An alternative definition has been proposed, stating that a lack of negative heat release (i.e. endothermic dominant reactions) occurs in MILD combustion conditions [44–46]. The negative heat release rate (HRR) definition is derived from opposed flow diffusion flames, increasing applicability from the PSR definition to include non-premixed turbulent flames [26,44]. This definition, however, is limited by the effects of strain rate, which can be difficult to quantify in experimental conditions [26]. Additionally, regime maps for classification need to be developed on a fuel-specific basis, limiting the generality [44]. A more recently published definition based on the equivalent activation energy of a single-step oxidation derived from an idealised flamelet analysis has been proposed [43]. This activation energy approach is derived from the single-step oxidation analyses of Peters' group [47–50], and of the canonical Burke–Schumann irreversible single-step flame [51]. The activation energy approach states that a monotonic S-shaped curve is indicative of MILD combustion, as there are no distinctive ignition or extinction phenomena under this condition. This analysis is agnostic to the fuel type and flow conditions, much like the negative heat release definition. When considering the flamelet theory for non-premixed turbulent combustion, or indeed laminar combustion, the activation energy definition is not limited by flame type [43]. However, determination of the activation energy for specific fuels at the required conditions is non-trivial, as the estimation condenses the detailed chemistry into a single-step, which is not valid across all conditions, especially given the importance of finite-rate chemistry in MILD combustion conditions [52–55]. Whilst the activation energy definition shares the limitation of fuel specific applications with the HRR definition, it is often defined through stoichiometric conditions, which are usually well known, or easily calculated for most fuels.

Estimation of global activation energy for the oxidation of a fuel has previously been conducted. A global mechanism for hydrogen combustion in air was developed through a best-fit process for laminar flame speed, with good agreement at equivalence ratios from 0.55–1.1 [56]. Another single-step hydrogen–air oxidation mechanism was developed from conservation equations for a reacting species for use in spark-ignition computations [57–59]. The reaction order and activation energy were estimated through an iterative approach to approximate gradients in density and temperature with initial conditions, resulting in constant values for different hydrogen dilutions. Excellent agreement with laminar flame speed and flame temperature were obtained using this method, however, low-oxygen, high-temperature conditions were not assessed, nor were elevated pressure conditions [57–59]. A similar analysis has been undertaken, however, a virtual species is included to take the place of the intermediate species for hydrocarbon–air combustion [60]. Whilst high-temperature combustion was considered, low-oxygen dilution conditions were not [60]. The optimisation strategy in this approach is through the fuel–air ratio, rather than an oxidant concentration approach, as with further work by this group on optimised two-step kinetics [60,61]. A single-step chemical mechanism for hydrogen has been validated for hydrogen concentrations from 12%–70% combusting in air, with good agreement for temperature prediction and laminar flame speed [62]. Reactant orders for the typical Arrhenius expression were fitted from experimental data [62]. A single-step model for hydrocarbon combustion in air was developed, using heat release, unburnt temperature, and pre-exponential factor as inputs [63]. However, it was found that the activation temperature varied significantly across equivalence ratios, resulting in a functional fit for activation temperature which becomes invalid in rich flames [63]. Challenges still remain in determining *a priori* the pre-exponential factor and heat release for use in this model. A similar reduction process was used to determine a reduced mechanism for hydrogen combustion in air, with accurate results in lean flames [64]. Development of a single-step model by implementation of a "virtual chemical mechanism" has also shown promise for prediction of activation energy and Arrhenius coefficients [65,66]. However, thermochemical properties of the products required separate fitting to meet the properties of the detailed mechanism being emulated [65,66]. Chemical kinetics reduction methods have also resulted in "global" mechanisms, consisting of one-, two-, or three-step mechanisms [67–71]. In particular, systematic reduction for a hydrogen–air combustion system resulted in a mechanism capable of predicting peak temperatures and flame propagation in a number of flame types [70]. Alternatively, eigenvalue analysis for chemical mechanism reduction has resulted in accurate recreation of explosion limits in hydrogen–ammonia homogeneous mixtures at different pressures, although the oxidant in this case is air, rather than low-oxygen combustion products [72]. Some extension of a reduced hydrogen–air mechanism has been performed, increasing the validity across a wider stoichiometric range, however, does not capture autoignition behaviour [73]. Despite the "global" moniker, the initial conditions for which these mechanisms are valid do not encompass all conditions relevant to combustion.

One of the challenges of combustion simulation is the significant computational requirements for solving species conservation equations, with computation time scaling typically with the cube of species number [74]. As such, development of generalised global mechanisms that retain accuracy whilst providing a computational time reduction is a key research focus. Both multi- and single-step mechanisms have been employed to assess the effect of pressure on stability of premixed flames [75]. It was found that with appropriate integration of the multi-step results, the single-step mechanism is capable of predicting the change of unstable length scale for premixed flames with pressure [75]. Stability from thermo-acoustic perturbations has also been investigated using single-step hydrogen kinetics, helping to demonstrate the impact of the coupling between hydrodynamics and acoustics on flame stability [76]. A single-step mechanism for hydrogen oxidation was used to test new methods time-scale evaluation of chemical kinetics, demonstrating the use of progress variables in characterising the time-scale of a reacting system [77]. Application of single-step mechanisms have been used in investigation of manifold parameterisation for *a priori* flame prediction, finding good agreement with species mass fraction and temperature predictions when compared with detailed chemistry [78]. Several global mechanisms have been used to investigate MILD oxy-combustion of methane, finding a four-step

mechanisms which adequately represented the species fractions and temperatures [79]. Similar analysis of global mechanisms for methane oxy-fuel combustion have also demonstrated success in simulation using a two-step mechanism modified for the oxy-fuel conditions [80]. The effects of preferential diffusion, a phenomena particularly notable in hydrogen flames, have been assessed using single-step kinetics for lean hydrogen–air and propane–air oxidation [81]. Flame stretch due to strain rate is well captured, as is flame thickness in 1D premixed flamelets [81]. Although significant research efforts have involved the use of single-step chemistry for modelling and stability analysis of a number of flames, a generalised single-step reaction mechanism that is valid across conditions including low-oxygen dilution, high-temperature, elevated pressure combustion, as well as conventional configurations has not been developed.

Single-step chemistry still remains an important feature of combustion analysis, both from a computational and theoretical perspective. However, a functional form of single-step Arrhenius rate coefficients, valid across a range of high-temperature, low-oxygen, and elevated pressure conditions, which can be used for modelling and theory analysis has not been proposed at this stage. Development of a single-step mechanism that is applicable across a range of conditions would allow for the computational advantages of a reduced mechanism, with the high fidelity temperature and heat release predictions of a detailed mechanism. This paper aims to outline development and testing of a method for estimation of global activation energy, and by extension, develop functional forms of the Arrhenius coefficients for several fuels across a range of conditions. The purpose of these functional Arrhenius coefficients will be to allow improved single-step modelling of combustion in low-oxygen, elevated temperature conditions, encompassing, but not limited to, those required for MILD combustion. The method proposed differs from previous single-step chemistry approximations by approaching the optimisation through parameters relevant to MILD combustion, such as oxidiser oxygen fraction, and initial temperature. In addition, the initial activation energy and pre-exponential factor are determined via a progress variable approach without high activation energy asymptotic analysis, treating the system globally in the governing equation.

2. Method and theory

2.1. Estimation of the global one-step activation energy

The process used for estimation of the Arrhenius rate coefficients of a single-step oxidation reaction is derived from the conservation equations of a reacting flow. The full derivation process is captured in Supplementary Material, Section A. A progress variable approach is used to approximate the global oxidation reaction. The progress variable (P), coupled with the species conservation equation, gives rise to the relationship in Eq. (2.1):

$$T \ln k_P = T \ln \left(\frac{\rho}{W_P} \frac{dP}{dt} [X_{C_xH_y}]^{-r_1} [X_{O_2}]^{-r_2} \right) = T \ln A - \frac{E}{R} \tag{2.1}$$

where k_P is the global reaction rate, T is the mixture temperature, ρ is the mixture density, W_P is the molecular weight of the progress variable, $[X_{C_xH_y}]$ is the molar concentration of the fuel, $[X_{O_2}]$ is the molar concentration of oxygen, r_j are the reactant orders, A is the Arrhenius rate pre-exponential factor, E is the Arrhenius rate activation energy, and R is the universal gas constant (8.314 J/mol/K). Data from simulations of detailed chemical kinetics can then be fitted using a least-squares method of linear regression to Eq. (2.1) to estimate values of A and E, using reaction orders that minimise Eq. (2.2)

$$L = (1 - \overline{GOF}) + \sigma(GOF) + (1 - \min(GOF)) \tag{2.2}$$

where GOF refers to the typical coefficient of determination, often denoted R^2. GOF is instead chosen to minimise confusion with R, the universal gas constant. The estimation of A and E from the described method can then be extended further by inclusion of the temperature modifying term in the modified Arrhenius rate equation, b, as in Eq. (2.3) [82]

$$k = AT^b \exp\left(-\frac{E}{RT}\right) \tag{2.3}$$

The initial estimates of A and E obtained can then be implemented in a statistical approach to determine an appropriate value of b to achieve agreement with quantities of interest (QoIs), in particular the ignition delay. The values of b are bounded by the typical orders of magnitude of the temperature exponent in detailed kinetic mechanisms (−10 to 10).

2.2. Computational work

2.2.1. Closed homogeneous batch reactors

Zero-dimensional batch reactor simulations were conducted using the CHEMKIN Pro AURORA subroutine. This subroutine solves the well-known conservation equations for a reacting system, assuming all spatial variables to be zero, resulting in a time-varying homogeneous system. Combustion of methane and hydrogen with low-oxygen hot oxidants were studied. In particular, a stoichiometric mixture of fuel and oxidant was simulated, where the oxidant consisted of the major products of fuel-lean combustion of 1:1 by mole H_2/CH_4 with air (N_2, O_2, CO_2, H_2O). The role of radicals in MILD combustion conditions has been shown previously to be significant [83–88]. However, much of the radical species influence is absorbed by modification of the Arrhenius coefficients for the required conditions, accounting for their effects implicitly, without explicitly transporting the species, or representing them through a surrogate or virtual species. Were the oxidiser changed to include intermediates, then the proposed fitting method would need to be applied to the new initial conditions. Similarly, the thermochemistry has not been modified to account for the intermediate species, unlike other optimised single-step chemistry approaches [60,61,65].

Selection of the detailed mechanism to use in the estimation process plays a more significant role than the oxidiser radical presence, requiring that the validation of the overall mechanism is high for the specific fuel being analysed. The GRI-Mech 3.0 kinetic mechanism was used to simulate the detailed chemistry cases [89]. Three other mechanisms (AramcoMech 3.0 [90], San Diego (2016-12-14) [91], and Polimi C_1–C_3 (March 2020) [92–94]) were investigated for use with methane and hydrogen. Although some minor differences were noted between the mechanisms for activation energy estimation and pre-exponential factor estimation, the features of the profiles retain similarity. GRI-Mech 3.0 and AramcoMech 3.0 in particular predicted activation energy and pre-exponential factors on the order of those seen in other single-step mechanisms in previous studies [43,64,67,95–97]. Due to its effectiveness in detailed simulation of hydrogen and methane, GRI-Mech 3.0 was selected for all further discussion of these fuels. The results of these mechanisms are presented in Supplementary Material Section A.3. The Polimi C_1–$C_1$6 (March 2020) [92–94] mechanism was used for simulation of n-heptane. Oxidant oxygen concentration, initial temperature, and pressure were varied across 945 cases per fuel in the following ranges (inclusive of endpoints):

- Oxygen at 3, 4, 5, 6, and 9%, corresponding to typical MILD conditions
- Initial temperature from 700–1500 K, corresponding to typical MILD conditions (100 K steps)
- Pressure 1–25 atm, corresponding to potential sequential gas turbine conditions (20 logarithmic steps)

The ranges above indicate the validated ranges for the developed functional forms, and have not been validated outside of these ranges. In-simulation time was limited to 5 s, and cases where the ignition delay (as defined by the inflection point in the temperature profile) was more than 0.5 s were deemed non-reacting. This is consistent with previous classification of autoignition in flame calculations [23,84,98–100].

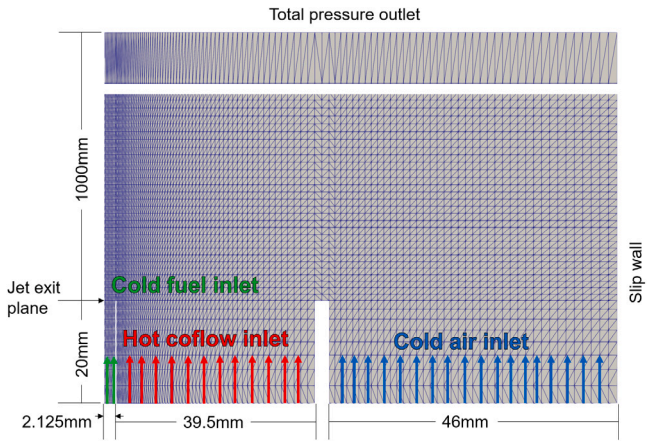

Fig. 1. Computational domain based on the JHC geometry [14] for CFD simulation of the tabulated flames in Table 2.

2.2.2. Opposed flow laminar flames

The CHEMKIN Pro OPPDIF subroutine was used to simulate a number of opposed flow diffusion flames using both detailed chemistry, and the estimated one-step global equations. Global strain rate, as defined by $a = (v_f + v_{ox})/L$, where subscripts f and ox refer to the fuel and oxidiser streams, respectively, was varied logarithmically from $1\,s^{-1}$ to $10\,000\,s^{-1}$ over 100 steps. The velocities of each inlet were selected to result in equal momentum between both streams, such that a stagnation plane occurs approximately at the midpoint of the domain.

Pressure was varied across the same range as in the closed 0D homogeneous cases, whereas the temperature was varied only across the temperature ranges where autoignition was determined as part of the initial cases. The fuel inlet was kept at 300 K, whilst the oxidant temperature was through the temperatures above autoignition in the initial cases, typically between 900 K and 1500 K.

The composition of the oxidant stream consisted of N_2, O_2, H_2O, and CO_2, assuming complete fuel-lean combustion of 1:1 by mole H_2/CH_4 in air, as in the closed 0D cases. These conditions are consistent with previous JHC experiments that emulate MILD combustion conditions [5,14,23,28,43].

2.3. Computational fluid dynamics

2.3.1. Burner and domain

OpenFOAM 7 was used to analyse a JHC burner in an axisymmetric wedge domain [14]. The burner consists of a 4.25 mm inner diameter central jet. This jet is surrounded by an 82 mm inner diameter coflow, which in turn is shrouded by coflowing cold air at the same bulk velocity. The coflow is composed of fuel-lean combustion products from burning 1:1 by mole H_2/CH_4 with a mixture of N_2 and air upstream. Ratios and quantities of N_2 and air are varied to achieve the desired oxygen concentration in the coflow and desired temperature. The bulk velocity of the coflow, $\bar{U}_{coflow}$, is approximate 3.2 m/s, as is the wind tunnel air velocity. The central fuel jet consists of 1:1 by mole H_2/CH_4, exiting the jet with a bulk Reynolds number of approximately 10k. The computational domain is an axisymmetric wedge, beginning 20 mm upstream of the jet exit, and extending 1000 mm downstream. Radially, the domain extends to 100 mm, which captures the coflowing wind tunnel. The computational domain is shown in Fig. 1, and the mesh independence results are summarised in Table 1, showing that the results are within the asymptotic range.

Table 1
Mesh independence criteria for computational analysis, using a factor of safety of 1.25 for the grid convergence index.

Number of cells	27 500	61 700	137 000
GCI	–	0.0181	0.0057

2.3.2. Boundary conditions

The coflow composition was modelled as the primary products of fuel-lean combustion of 1:1 by mole H_2/CH_4 with air and N_2, namely N_2, O_2, H_2O, and CO_2. For the purpose of analysis, the jet was first modelled as in the JHC experiments [14], consisting of 1:1 by mole H_2/CH_4 to demonstrate accuracy of the GRI-Mech 3.0 mechanism to capture the main features of the flame when compared to experimental data. Following this validation, methane was removed from the jet, resulting in a single-fuel case that can be compared with the one-step global chemistry developed in this work. The burner operating conditions are summarised in Table 2.

Uniform profiles of velocity were defined at the inlets, based on the bulk Reynolds numbers reported in experiments [14].

2.3.3. Turbulence-chemistry modelling

A Reynolds-averaged Navier–Stokes turbulence modelling approach was used, with the two-equation k-ϵ turbulence closure model implemented. The $C_{1\epsilon}$ constant was modified to be 1.6 rather than 1.44 to improve round jet modelling, in accordance with previous studies [101], however, all other constants were maintained as in the original formulation.

The single-step chemical mechanism used was in the Chemkin format based on the Arrhenius coefficients for 3% and 9% X_{O_2}, at 1 atm, and 1200 K. As the simulations were constant pressure, no pressure dependency was implemented. However, for both OpenFOAM and ANSYS Fluent, user-defined functions can be implemented to allow the algebraic representation of the Arrhenius coefficients in order to adapt the reaction rates to the local conditions, rather than a constant global mechanism.

The turbulence-chemistry interactions were captured using the eddy dissipation concept (EDC) model, a finite-rate kinetics extension of the eddy dissipation model that is capable of resolving detailed chemistry including backward reaction rates [102,103]. The efficacy of EDC for MILD combustion has been shown to provide adequate results for JHC experiments [6,25,104–109]. The C_τ and C_ξ constants were modified to be 3 and 1, rather than 0.4082 and 2.1377, to better capture MILD combustion conditions, as in previous studies [6,25,53].

3. Results and discussion

3.1. Estimation of the single-step Arrhenius coefficients

Adequate representation of the progress variable is paramount in appropriately estimating a single-step reaction from the detailed mechanism. In order to be a valid representation, the progress variable must be related to the global one-step oxidation equation, either by participation (ideally as a product), or through a close chain-branch in the detailed mechanism that results in a stable intermediate. $P_{CH_4} = Y_{CO_2} + Y_{H_2O}$ was chosen for the progress variable for methane, whilst only $P_{H_2} = Y_{H_2O}$ was appropriate for hydrogen. The determination of reactant orders in the Arrhenius rate expression required a parametric variation of reactant orders for each fuel, minimising the cost function defined in Eq. (2.2). The results of the reactant order curve fitting are reported in Table 3.

A quasi-linear section of Eq. (2.1) was defined to evaluate the Arrhenius coefficients over the primary reaction time. The upper temperature endpoint was defined as the first local maxima of Eq. (2.1) before equilibrium. The low temperature point was defined as the point where the temperature–time curve radius of curvature was at

Table 2
Reported nominal operating conditions for initial JHC cases HM1-3 [14], and inlet conditions for pure hydrogen computational cases, H1 and H3.

Case	Coflow						Jet			
	$\bar{U}_{coflow}$ (m/s)	Y_{O_2}	Y_{N_2}	Y_{CO_2}	Y_{H_2O}	T (K)	Re_{bulk}	Y_{CH_4}	Y_{H_2}	T (K)
HM1	3.2	0.03	0.85	0.055	0.065	1300	10k	0.89	0.11	305
HM2	3.2	0.06	0.82	0.055	0.065	1300	10k	0.89	0.11	305
HM3	3.2	0.09	0.79	0.055	0.065	1300	10k	0.89	0.11	305
H1	3.2	0.03	0.85	0.055	0.065	1300	10k	0	1	305
H3	3.2	0.09	0.79	0.055	0.065	1300	10k	0	1	305

Table 3
Reactant orders determined using the process described in Section 2.1 as part of evaluation of Eq. (2.1).

Fuel	r_1	r_2
Hydrogen	2	2
Methane	1	0.425

Table 4
Coefficients of lines of best fit in Fig. 2, for the conditions $p_i = 3.09$ atm, $T_i = 1200$ K, and $X_{O_2} = 3$ and 9%, as well as coefficients of determination. The equation is of the form $T\ln(k_p) = T\ln(A) - E/R$, where R is the universal gas constant. GOF is the goodness-of-fit, using the typical coefficient of determination metric.

Fuel	A	E [J/kg]	GOF
Hydrogen (3%)	1.81×10^{40}	4.39×10^{5}	0.994
Hydrogen (9%)	6.22×10^{29}	2.05×10^{5}	0.997
Methane (3%)	1.49×10^{42}	9.32×10^{5}	0.948
Methane (9%)	1.36×10^{28}	6.14×10^{5}	0.959

a minimum, i.e. thermal runaway was beginning. Whilst defining the first local maxima before the equilibrium temperature does not result in perfect endpoints, the least-squares regression form of determining the pre-exponential factor and activation energy reduces the error introduced near the upper temperature endpoints. The quasi-linear section of Eq. (2.1) can be approximated by the Arrhenius rate equation. The coefficients of this approximation can be determined through a best-fit line using a least-squares regression. The result of the least-squares regression, as solid (3%) and dashed (9%) lines, is overlaid on the initial data (symbols, down-sampled), in Fig. 2 for example conditions of $p_i = 3.09$ atm, $T_i = 1200$ K, and $X_{O_2} = 3$ and 9%. Coefficients for the lines of best fit, as well as the GOF values are presented in Table 4. At 9% O_2, the estimated values of activation energy and pre-exponential factor are within an order of magnitude of other conventional single-step estimations for hydrogen and methane oxidation [43,67].

For hydrogen, Fig. 2 shows good correlation across the whole temperature range for both 3 and 9% O_2 mole fraction. However, methane shows better agreement at low temperature than at high temperatures, indicating hydrogen and methane progress variables result in differing trends as temperature increases. In addition, the complexity of the dissociation reactions at higher temperatures contributes to the non-linearity observed in this region, especially considering the over-simplification of the kinetics inherent in the single-step approximation. Reduction of oxygen concentration appears to have a lesser impact on the quasi-linear evaluation for hydrogen, however, the slope of the methane quasi-linear regions becomes higher, leading to lower activation energy evaluation.

The regression coefficients from the cases assessed, such as those in Table 4, result in several hundred values that can be generalised into a function form. A multivariate polynomial regression in three variables – oxygen concentration, initial temperature, and pressure – was determined for each Arrhenius coefficient. The result is two functions, one for the activation energy, and one for the pre-exponential factor. The functions are second order in oxygen concentration and temperature, and third order in the log of pressure. The general form of these equations are given as Eq. (3.1):

$$f(T_i, p_i, X_{O_2}) = c_0 + c_1 T_i + c_2 p_i + c_3 X_{O_2} + c_4 T_i^2 + c_5 T_i p_i + c_6 p_i^2 + c_7 T_i X_{O_2} + c_8 p_i X_{O_2} + c_9 X_{O_2}^2 + c_{10} T_i^2 p_i + c_{11} T_i p_i^2 + c_{12} p_i^3 + c_{13} T_i^2 X_{O_2} + c_{14} T_i p_i X_{O_2} + c_{15} p_i^2 X_{O_2} + c_{16} T_i X_{O_2}^2 + c_{17} p_i X_{O_2}^2 \quad (3.1)$$

Table 5
Multivariate polynomial regression coefficients in the form of Eq. (3.1), for prediction of activation energy in the Arrhenius rate expression.

Coefficients	$\log_{10}(A)$		E	
	H_2	CH_4	H_2	CH_4
c_0	509	7.74	3.68e+6	−2.99e+4
c_1	−0.507	7.68e−2	−3.93e+3	−296
c_2	−65.6	77.0	−1.13e+6	1.13e+6
c_3	−63.8	−8.78	−4.38e+5	−2.75e+4
c_4	1.42e−4	5.63e−5	1.05	1.52
c_4	0.191	−0.248	2.75e+3	−2.82e+3
c_6	−32.6	7.44	−4.09e+5	9.01e+4
c_7	5.64e−2	7.96e−3	329	130
c_8	−4.89	15.7	−2.7e+4	1.27e+5
c_9	2.90	−0.966	2.16e+4	−1.83+4
c_{10}	−8.34e−5	9.61e−5	−1.14	0.973
c_{11}	2.44e−2	−1.79e−2	339	−228
c_{12}	−0.542	7.25	−1.28e+4	8.14e+4
c_{13}	−9.28e−6	−1.85e−5	−3.00e−2	−0.278
c_{14}	−1.88e−3	2.93e−3	−37.2	67.3
c_{15}	0.406	−0.610	3.81e+3	−4.53e+3
c_{16}	−1.95e−3	2.02e−3	−13.8	28.3
c_{17}	0.377	−1.09	3.72e+3	−1.21e+4

The coefficients for each of the fuels, corresponding to c_0 through c_{17} in Eq. (3.1), are summarised for each fuel in Table 5, for the effective activation energy, $f = E$, and for the pre-exponential factor in logarithm form, $f = \log_{10}(A)$.

Extension of the modified Arrhenius rate expression results in inclusion of a temperature modifying term, b, as in Eq. (2.3). Although b can be fitted as part of the regression process used to determine A and E, an iterative approach for determining the temperature exponents for each condition was taken, optimising the values for ignition delay agreement with the detailed chemistry. A similar multivariate regression was performed to obtain a functional fit for the temperature exponent once an error of less than 1% was achieved in the ignition delay prediction. As the temperature exponent shows significantly greater non-linearity in the trends with changes in pressure as opposed to the activation energy and pre-exponential factors, the multivariate regression for b involved a fourth order pressure term. The form of this regression is shown in Eq. (3.2):

$$b(T_i, p_i, X_{O_2}) = c_0 + c_1 T_i + c_2 p_i + c_3 X_{O_2} + c_4 T_i^2 + c_5 T_i p_i + c_6 p_i^2 + c_7 T_i X_{O_2} + c_8 p_i X_{O_2} + c_9 X_{O_2}^2 + c_{10} T_i^2 p_i + c_{11} T_i p_i^2 + c_{12} p_i^3 + c_{13} T_i^2 X_{O_2} + c_{14} T_i p_i X_{O_2} + c_{15} p_i^2 X_{O_2} + c_{16} T_i X_{O_2}^2 + c_{17} p_i X_{O_2}^2 + c_{18} T_i^2 p_i^2 + c_{19} T_i p_i^3 + c_{20} p_i^4 + c_{21} T_i^2 p_i X_{O_2} + c_{22} T_i p_i^2 X_{O_2} + c_{23} p_i^3 X_{O_2} + c_{24} T_i^2 X_{O_2}^2 + c_{25} T_i p_i X_{O_2}^2 + c_{26} p_i^2 X_{O_2}^2 \quad (3.2)$$

Whilst many terms are similar to Eq. (3.1), some higher order terms are also determined. Table 6 presents the coefficients c_0 through c_{26} for the temperature exponent regression.

Table 6
Multivariate polynomial regression coefficients in the form of Eq. (3.2), for prediction of temperature exponent in the Arrhenius rate expression.

Coefficients	b	
	H_2	CH_4
c_0	9.51	−13.5
c_1	−1.66e−2	2.42e−2
c_2	13.9	−10.6
c_3	−4.76	4.72
c_4	6.90e−6	−1.04e−5
c_4	−2.04e−2	1.28e−2
c_6	−5.22	4.17
c_7	8.00e−3	−8.47e−3
c_8	−0.372	1.29
c_9	0.322	−0.316
c_{10}	7.33e−6	−3.41e−6
c_{11}	1.00e−2	−8.01e−3
c_{12}	−0.834	0.685
c_{13}	−3.32e−6	3.67e−6
c_{14}	−1.36e−4	−4.19e−4
c_{15}	0.196	−4.79e−3
c_{16}	−5.49e−4	5.83e−4
c_{17}	4.13e−2	−0.151
c_{18}	−4.35e−6	3.47e−6
c_{19}	6.05e−4	−5.07e−4
c_{20}	−1.26e−2	−4.78e−3
c_{21}	3.49e−7	−4.21e−7
c_{22}	−1.88e−4	2.64e−5
c_{23}	1.96e−2	8.57e−5
c_{24}	2.30e−7	−2.57e−7
c_{25}	−3.13e−5	1.14e−4
c_{26}	−1.89e−3	−4.40e−4

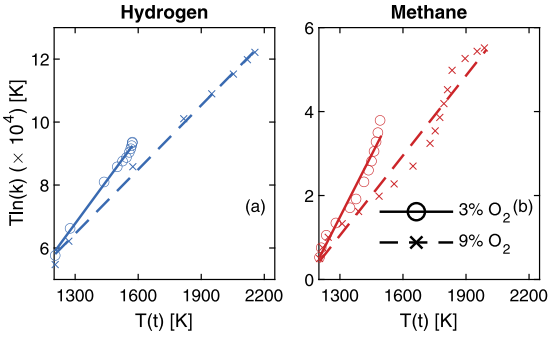

Fig. 2. Fitted functions for the quasi-linear region of governing equation. Conditions of $p_i = 3.09\,\text{atm}$ and $T_i = 1200\,\text{K}$, with $X_{O_2} = 9\%$. Coefficients for lines of best fit ($T\ln(k) = T\ln(A) - E/R$) are summarised in Table 4. To improve visibility, only every fifth marker is shown.

3.2. Dependence of activation energy estimation on different variables

Pressure has a direct influence on the chemical kinetics, through a combination of pressure-dependent reactions, and through the activation volume property [110–112]. Fig. 3 shows the relationship between pressure and the Arrhenius coefficients at several temperatures, for $X_{O_2} = 9\%$.

Fig. 3 indicates that when the temperature of methane reactants is increased, both the pre-exponential factor and activation energy tend to increase. Conversely, both coefficients decrease when hydrogen is the fuel. Both progress variables are monotonic with temperature across all conditions assessed, thus the differences in the pre-exponential factor and activation energy trends are attributed to fundamental changes in the chemistry between the fuels. Analysis of the effects of temperature on the reaction pathways of diluted methane has previously shown the complex behaviour of methane in this regime that is reflected in Fig. 3 [54,113–115]. Previous single-step Arrhenius rate estimations have shown increases in predicted activation energy for hydrogen

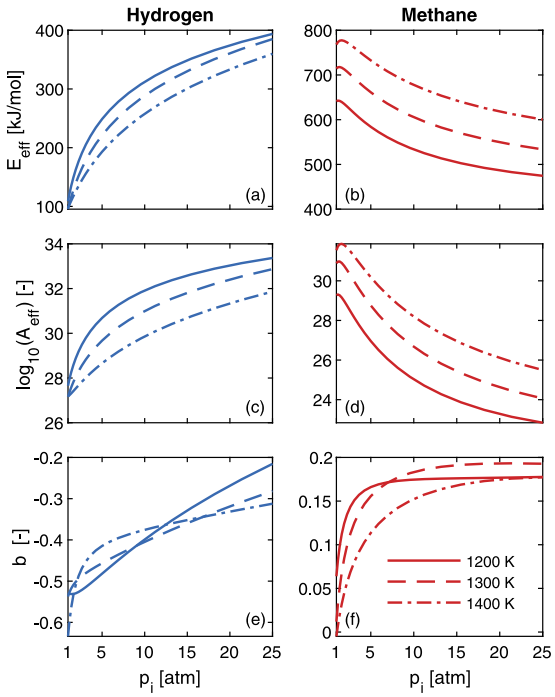

Fig. 3. Plots showing examples of the relationship between initial pressure and Arrhenius coefficients for $T_i = 1200\,\text{K}$, $1300\,\text{K}$, and $1400\,\text{K}$, at a fixed oxidant concentration of $X_{O_2} = 9\%$. (a–b) Effective activation energy, (c–d) base 10 logarithm of the pre-exponential factor, (e–f) temperature exponent.

as pressure increases, and decreases for methane with increases in pressure [95–97].

The trends of temperature exponent, b, with changes to initial temperature in Fig. 3 appear to oppose those of the pre-exponential factor and activation energy for hydrogen. That is, where an increase in temperature results in a decrease in activation energy for hydrogen, it results in an increases in temperature exponent instead. The relationship between pressure and temperature exponent for hydrogen follows the higher-order polynomial features more so than methane. The morphology of the temperature exponent for both fuels shows a crossover in exponent values, indicating a reversal in the trends with a change in temperature.

Higher temperature exponent tends to result in faster ignition, as the reaction is accelerated. The magnitudes of temperature exponent differ greatly between the fuels, however, so too do the pre-exponential factor and activation energies. Given the typical slower ignition delay of methane [116], the higher temperature exponent prediction relative to hydrogen likely results from the intrinsic chemistry that this method is approximating, rather than an artefact of the methodology used. The highly non-linear relationship between pressure and temperature exponent likely comes as part of the balance between the pre-exponential factor and activation energy as pressure increases. In the case of hydrogen, increasing pressure results in an increase in pre-exponential factor, but also activation energy, resulting in more collisions per unit time, but less successful ones, proportionally. Given the exponential relationship that both A and E have on the rate of reaction, the iterative approach to determining b results in a non-linear relationship to balance A and E.

Oxygen concentration was also varied, and the impact of this variation on the Arrhenius coefficients is shown in Fig. 4. For methane, changes in O_2 mole fraction have the opposite effect on pre-exponential factor and activation energy than what was observed for changes in temperature in Fig. 3. Increases in O_2 tend to decrease both activation energy and pre-exponential factor, appearing to collapse towards a single line at elevated O_2, whereas increases in temperature of the

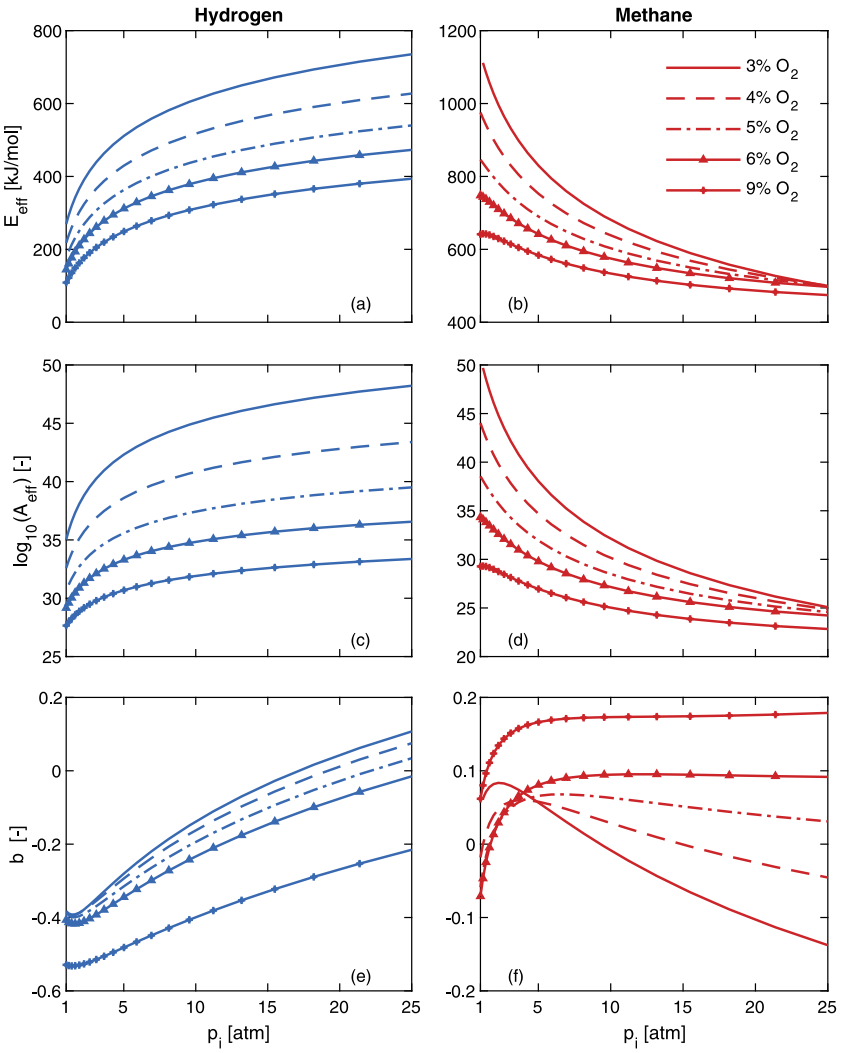

Fig. 4. Plots showing examples of the relationship between initial pressure and Arrhenius coefficients for $X_{O_2} = 3\%$, 4%, 5%, 6%, and 9%, at a fixed temperature of $T_i = 1200\,\mathrm{K}$. (a–b) Effective activation energy, (c–d) base 10 logarithm of the pre-exponential factor, (e–f) temperature exponent.

reactants results in an increase in both coefficients. Hydrogen, however, decreases in pre-exponential factor and activation energy with an increase in either temperature or O_2 mole fraction. The morphology of the pre-exponential factor and activation energy with changes in O_2 remains similar, as with the changes in reactant temperature.

Similar to the changes in reactant temperature, changes in O_2 result in large variations in the morphology of the b–p_i curves for methane. In Fig. 4(e), hydrogen shows only a change in magnitude for b, with minimal effect on the morphology, suggesting a transition in behaviour of the global ignition is more contingent on the initial temperature rather than oxidant availability. Comparatively, in Fig. 4(f), methane exhibits a significant difference in temperature exponent at reduced O_2, resulting in a large decrease to negative exponent values. As discussed in regards to the effect of changing reactant temperature, the temperature exponent balances out the non-linear contributions of the estimated activation energy and pre-exponential factors to optimise ignition delay. As both activation energy and pre-exponential factor vary non-linearly themselves, the resulting temperature exponent shares highly non-linear characteristics.

It is also noted that the relationship between oxygen level and temperature exponent at low pressures in Fig. 4(f) shows very non-linear behaviour with changes in oxidant. Fig. 5 shows the relationship between oxygen level and temperature exponent for methane at a 1 atm of pressure and several initial temperatures. At low pressures, the logarithm of pressure approaches 0, resulting in the multi-variate regression relationship of Eq. (3.2) collapsing into a bi-variate second-order regression. As such, the relationship observed in Fig. 5 appears parabolic, causing significant differences in the exponent for different oxygen levels in methane. Whilst this is not observed in the case of hydrogen in Fig. 4(e), extension below or above the oxygen ranges evaluated would depict this behaviour.

3.3. Validation against detailed chemistry

3.3.1. Ignition delay and equilibrium temperature

To assess the validity of the proposed single-step mechanism using functional Arrhenius coefficients, two main parameters in homogeneous batch reactor performance were assessed: ignition delay and equilibrium temperature. Due to the temperature conditions being above auto-ignition (see Section 2.2.1), laminar flame speed is no longer an appropriate metric for evaluating the kinetics, and hence is not considered [117]. Ignition delay and equilibrium temperature indicate whether finite-rate chemistry effects, and species thermochemical properties are being well represented. Closed homogeneous batch reactor simulations were conducted using the single-step mechanisms based on the predicted Arrhenius coefficients, and the resulting ignition delays and equilibrium temperatures were compared against the values obtained using the detailed mechanisms. Fig. 6 shows comparisons of ignition delay between the single-step and detailed mechanisms for the

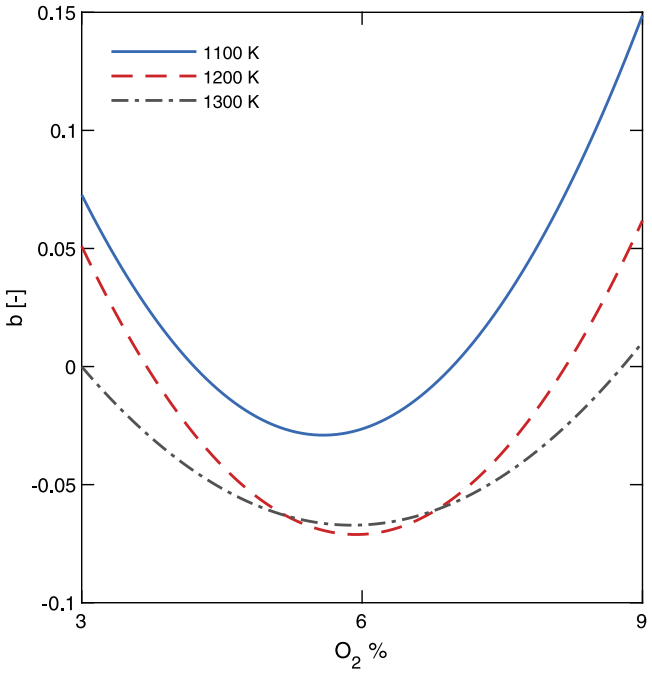

Fig. 5. Relationship between O_2 and temperature exponent at different initial temperatures and a fixed pressure of 1 atm for methane.

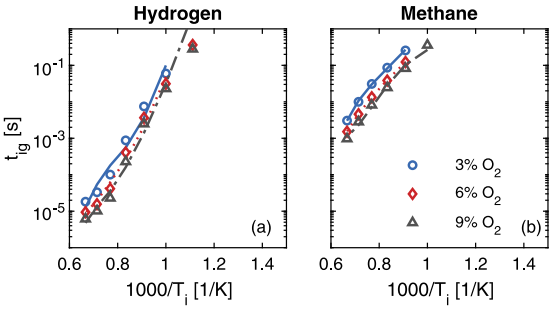

Fig. 6. Ignition delay (t_{ig}) prediction as a function of initial temperature (T_i) using the single-step global mechanisms for X_{O_2} = 3%, 6%, and 9%, at a fixed pressure of p_i = 5 atm. Symbols are derived from the detailed simulations, whereas as the dotted–dashed line is from one-step kinetics.

0D closed homogeneous batch reactors at three O_2 levels, and at a fixed pressure of 5 atm. Pressures of 1.2, 3.1, 11, and 25 atm are shown in Supplementary Material, Section B.1, however, the general behaviour exhibited remains the same.

The predictions of ignition delay show very good agreement between the detailed and single-step mechanisms. At lower temperatures, ignition delay for single-step hydrogen mechanisms is over-predicted, however, there is strong agreement for elevated temperature conditions (i.e. above 1000 K). Comparatively, methane shows excellent agreement between single-step and detailed predictions of ignition delay across all initial temperatures. It is suggested that the intermediate chemistry in hydrogen is more sensitive to changes in initial conditions, thus reducing the accuracy of estimation of a single-step mechanism. The ignition ranges for each fuel are also captured, with minimal low temperature ignition occurring for methane in both the detailed and single-step chemical mechanisms. It should be noted that while methane will still ignite at temperatures slightly lower than 1000 K, the ignition delay definition used here requires this time frame to be less than 0.5 s (refer Section 2.2.1).

Equilibrium flame temperature is another quantity of interest to represent whether the one-step approximation is appropriate and valid.

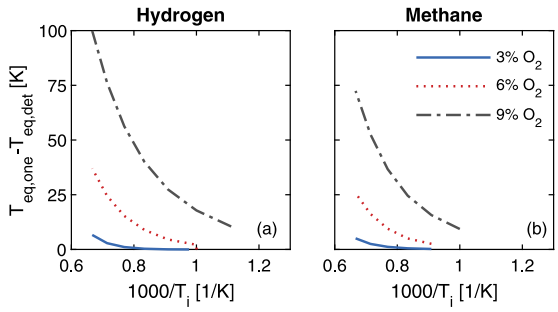

Fig. 7. Final temperature difference ($T_{eq,one} - T_{eq,det}$) between detailed and single-step mechanisms. The prediction is a function of initial temperature (T_i) for X_{O_2} = 3%, 6%, and 9%, at a fixed pressure of p_i = 5 atm.

Fig. 7 shows the difference between the final temperatures of the one-step and detailed simulations at 5 atm. Subscripts *eq*, *one*, and *det* in Fig. 7 refer to equilibrium, one-step, and detailed mechanisms, respectively. Increases in the reactant temperature result in a greater over-prediction of equilibrium flame temperature across both fuels and all O_2 levels. Similar trends are also observed at all pressures, as shown in Supplementary Material, Section B.2 for brevity. Both fuels show very similar behaviour when varying initial reactant temperature, and when varying the oxygen content. Low O_2 combustion results in the closest approximation of equilibrium flame temperature, whilst higher O_2 increases discrepancies, especially at higher initial reactant temperature. At 3% O_2, the over-prediction in temperature is negligible, but becomes significant at 9% O_2, especially at reactant temperatures above 1200 K.

In the single-step mechanisms, pyrolysis of the fuels is not captured, resulting in a higher heat release rate, and subsequently higher temperature prediction when compared with the detailed mechanisms. Additionally, stable intermediates which absorb heat energy are not present in the single-step mechanisms, resulting in a slight increase in the predicted temperature. At higher O_2, heat release is higher, and the lack of intermediate species and subsequent endothermic reactions due to their presence is likely to result in the greater over-prediction of adiabatic temperature in these conditions when compared with the low O_2 cases. Regardless, temperature remains well predicted in the low reactant temperature range for all conditions and fuels.

Species consumption shows agreement for oxidiser and fuel alike, with consumption plots presented in the Supplementary Material Section B.3 for brevity.

3.3.2. Sensitivity of temperature and ignition delay to Arrhenius coefficients

To evaluate robustness of the functional form of the Arrhenius coefficients, sensitivity of ignition delay and final temperature to changes in each coefficient is evaluated. Fig. 8 shows of sensitivity of hydrogen ignition delay to changes in E, A, and b for at 9% O_2. The y-axes of the colour maps indicate the percentage change in each Arrhenius coefficient, whilst the other two are held constant at the initial predicted value. The colour scale itself signifies the difference in ignition delay between the unchanged single-step mechanism prediction of ignition delay, and the prediction of ignition delay based on a percentage change in one of the Arrhenius coefficients, i.e. $\Delta t_{ig} = 100 \times (t_{mod,ig} - t_{orig,ig})/t_{orig,ig}$. Subscripts *mod* and *orig* refer to the case where an Arrhenius coefficient is modified, and where it is not modified, respectively. A corresponding figure to Fig. 8 for methane may be found in Supplementary Material, Section C.1.

Fig. 8 shows that the sensitivity of ignition delay to both activation energy and temperature exponent is significant. Pre-exponential factor appears to have a very limited effect on ignition delay, except at the extremes of ±25% variation, where a maximum of 25% change in ignition delay is observed. Comparatively, changes to activation energy

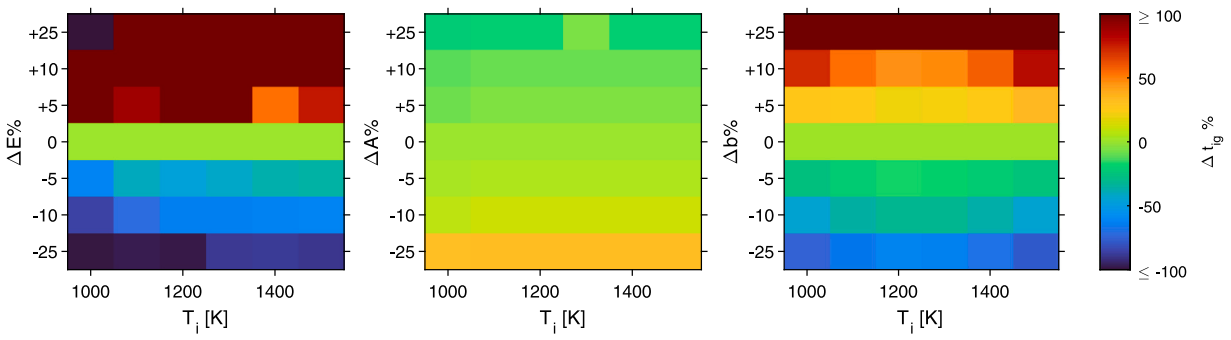

Fig. 8. Sensitivity of ignition delay to imposed changes in activation energy (E), pre-exponential factor (A), and temperature exponent (b) at an oxygen content of $X_{O_2} = 9\%$ and $p_i = 1$ atm. The fuel used is hydrogen. Subscript ig refers to ignition. Note that the colour limits are reduced to better portray the limits of sensitivity. (For interpretation of the references to colour in this figure legend, the reader is referred to the web version of this article.)

result in significant changes to the predicted ignition delay, with as little as 5% increase in E causing greater than 100% increase in ignition delay. As expected, at lower temperatures, Fig. 8 shows that negative changes in activation energy result in a reduction in ignition delay, but positive changes increase ignition delay. At elevated temperatures, this effect becomes less apparent, resulting in less sensitivity of ignition delay to effective activation energy. As such, accurate estimation of the activation energy becomes paramount for adequate representation of the detailed kinetics as a single-step mechanism, especially with low temperature ignition.

In the case of varying the temperature exponent, increases to the magnitude of the value will increase the ignition delay time, as most temperature exponents are negative. Similarly, decreasing the magnitude will result in an decrease in ignition delay time. The ignition delay time remains relatively insensitive to small changes in temperature exponent however, with less than 25% change to ignition delay time when varied by ±5%.

Sensitivity to the final temperature was also assessed, finding that there was less than 5% difference across all pressures, oxygen levels and temperatures for hydrogen when varying the Arrhenius coefficients by the same margins as presented in Fig. 8. Methane displayed similar characteristics, however, increases in activation energy tended to result in no ignition, hence a significant reduction in predicted equilibrium temperature. However, at elevated pressures, similar trends to those described for hydrogen were observed. Colour maps as in Fig. 8 may be found in Supplementary Material, Section C.2 for final temperature sensitivity.

3.3.3. Extension to large hydrocarbons

Whilst not explored extensively in this work, the proposed method can be extended to larger hydrocarbons, with *n*-heptane chosen as an example. The Polimi C_1–C_{16} mechanism [92–94] was selected for use as the detailed mechanism due to its strong validation against *n*-heptane combustion. Using the same process as described in Section 2.1, reactant orders of 1.7 and 0.0477 were determined for O_2 and *n*-heptane, respectively. Comparisons of ignition delay and temperature differences for *n*-heptane between the single-step and detailed kinetics are shown in Fig. 9. The results of the fitting functions are presented in Supplementary Material, Section A.4.

The ignition delay characteristics of *n*-heptane are known to show negative temperature coefficient (NTC) behaviour, whereby lower temperature ignition delay is less than the ignition delay at higher temperatures [118–120]. NTC behaviour is captured using the function Arrhenius coefficient form, as seen in Fig. 9(a) at all oxygen levels. Additionally, the temperature over-prediction in these conditions is minimal, with less than 100 K over-prediction seen in Fig. 9(b), comparable with the over-prediction in hydrogen and methane flames observed in Fig. 7.

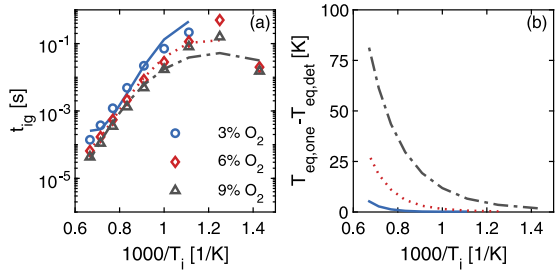

Fig. 9. (a) Comparison of ignition delay (t_{ig}) as a function of initial temperature between detailed and single-step kinetics for *n*-heptane. (b) Difference in equilibrium temperature between detailed and single-step kinetics for *n*-heptane. The pressure is $p_i = 5$ atm.

3.3.4. Temperature and heat release profiles in opposed flow laminar flames

A series of opposed flow hydrogen laminar flames were analysed to investigate the accuracy of the single-step estimation in capturing the features of a one-dimensional flame. Fig. 10 shows the temperature profiles and heat release profiles in mixture fraction space of both a detailed and single-step hydrogen kinetic mechanism for $T_i = 1300$ K, $p_i = 5$ atm, and $X_{O_2} = 6\%$, across at 25–1000/s global strain rate.

Fig. 10(a–d) show that temperature profiles in mixture fraction space for single-step chemistry are in excellent agreement with the detailed chemistry. Towards the fuel-rich side of the flame, some over-prediction of temperature is noted in the single-step mechanism, a feature that can be attributed to the lack of fuel pyrolysis being captured, much like that of the closed 0D batch reactor simulations. This is also evident in the heat release profiles, where the fuel-rich zone shows a slight over-prediction in amplitude for the single-step chemistry. Despite this, the heat release profiles in Fig. 10 across all strains are very well captured.

As with the 0D batch reactor cases, species consumption shows agreement for oxidiser and fuel alike, with consumption plots presented in the Supplementary Material Section D.1 for brevity.

3.3.5. Behaviour approaching extinction strain rate

Capturing the behaviour close to extinction strain is important in demonstrating the capacity of the single-step mechanism for simulating all flow regimes. Increasing strain rate beyond that shown in Fig. 10, hydrogen flames approach extinction. The peak temperature can be plotted with strain rate between the single-step and detailed kinetics, to compare how well behaviour approaching extinction is captured. Fig. 11 shows an example of the peak temperature with different strain rates for the case of $T_i = 1200$ K, $p_1 = 1$ atm, and $X_{O_2} = 9\%$.

As strain rate increases, the trend of predicted peak temperature for the single-step mechanisms in Fig. 11 closely follows that of the detailed mechanism. At strains approaching extinction for the detailed

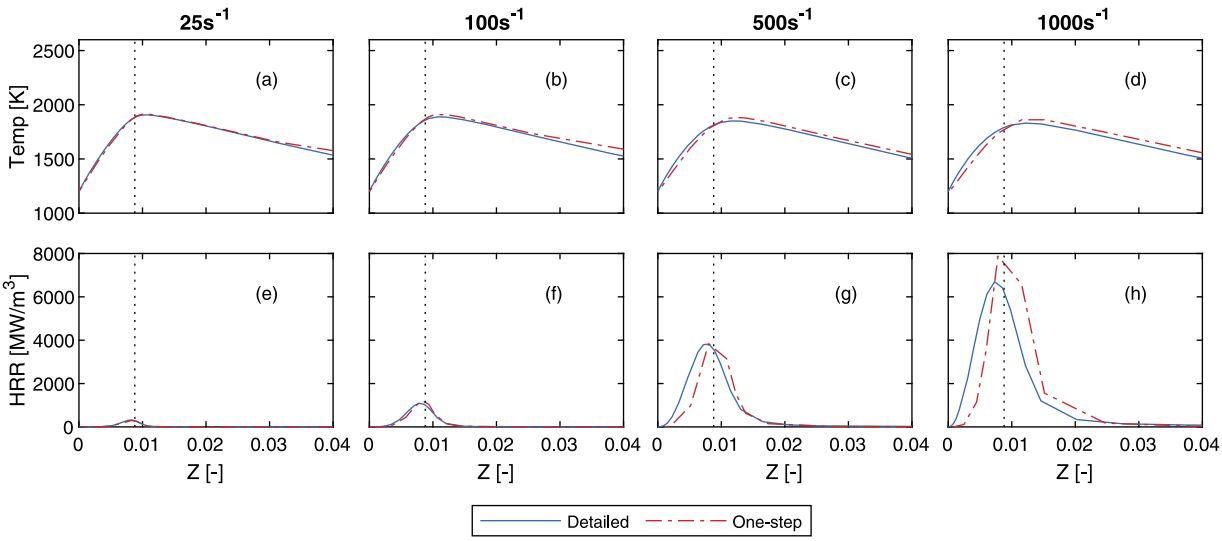

Fig. 10. Temperature and heat release profiles of detailed and one-step opposed flow laminar diffusion flames, at $T_i = 1200\,\mathrm{K}$, $p_i = 5\,\mathrm{atm}$, $X_{O_2} = 6\%$, and 25–1000/s global strain. The dotted vertical black lines indicate the stoichiometric mixture fraction. (a–d) Temperature profiles. (e–g) Heat release profiles.

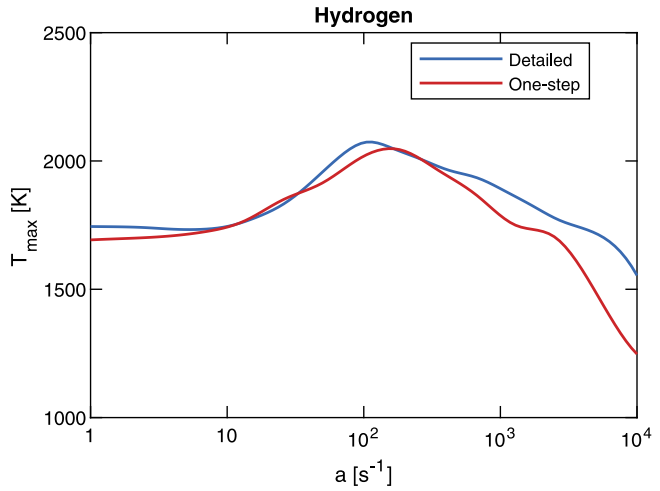

Fig. 11. Trends of peak temperature with strain rate approaching extinction for hydrogen opposed flow laminar flames at $p_i = 1\,\mathrm{atm}$, $T_i = 1200\,\mathrm{K}$, and $X_{O_2} = 9\%$.

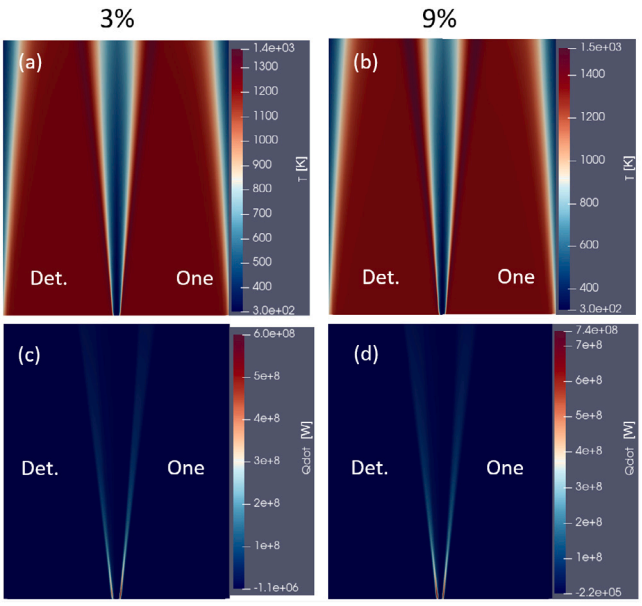

Fig. 12. Comparison of temperature and heat release between detailed and one-step chemistry for a hydrogen jet flame at 9% coflow O_2 mass fraction, with conditions derived from [14]. (a–b) Temperature images, (c–d) heat release rate images.

mechanism, peak temperature reduces significantly for the detailed mechanism, but reduces even more so for the single-step mechanism. Despite the decrease in peak temperature, the trends of peak temperature when strain is varied match well with the detailed mechanism, suggesting that flames with high local scalar dissipation rates could still be modelled using a single-step mechanism that adequately captures the temperatures of these flames. Extinction strain rate for both the detailed and single-step mechanisms was determined to be just above a global strain rate of $10\,000\,\mathrm{s}^{-1}$, with no ignition observed at $10\,300\,\mathrm{s}^{-1}$ for either mechanism.

3.4. CFD modelling of JHC type flames

3.4.1. Temperature and heat release prediction

Computational fluid dynamics simulations using OpenFOAM 7 were conducted to compare the capacity for the single-step mechanism in capturing key flow features with that of the detailed kinetics. Fig. 12 shows temperature predictions and heat release profiles compared between the single-step kinetics and detailed kinetics for a pure hydrogen jet with a bulk mean jet Reynolds number of 10 000, issuing into a coflow. The coflows have oxidant mass fractions of 3 and 9% (Y_{O_2}), and have a temperature of 1300 K.

At both 3 and 9% O_2, the flame shape is well captured, as are the peak temperatures in the flame sheet. Broadening of the reaction zone can be observed through the peak temperature images, with similar rates in detailed and single-step kinetics alike. Whilst the location of heat release rate in Fig. 12(c–d) is similar, the amplitude is greater near the jet exit from the single-step mechanism. This again is similar to that observed in both the closed 0D batch reactors and opposed flow diffusion flames, where fuel pyrolysis plays a role in the reduction of heat release rate in detailed mechanisms, which cannot be captured in the single-step mechanisms. Downstream, heat release shows better agreement between detailed and single-step chemistry. Radial profiles of both heat release and temperature are shown in Fig. 13 at several heights above the jet exit plane.

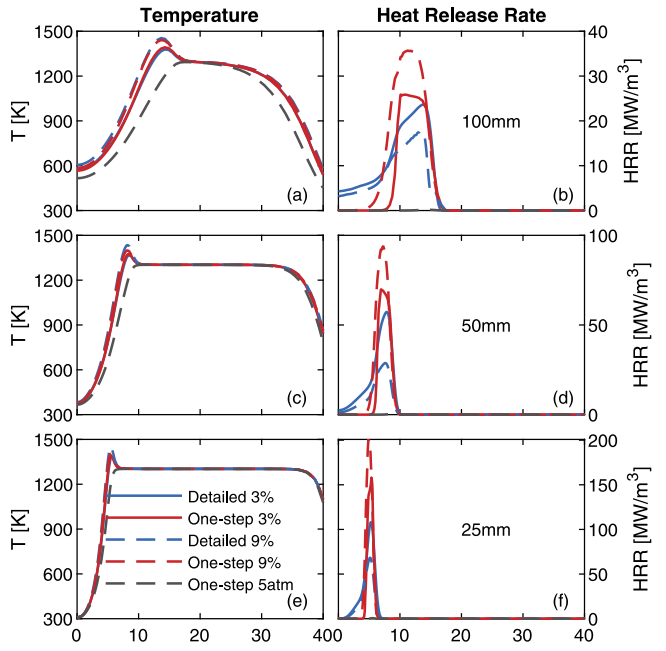

Fig. 13. Radial profiles of temperature and heat release rate using the detailed GRI 3.0 mechanism, and the one-step chemistry developed here for 3% and 9% Y_{O_2}, at heights of 25, 50, and 100 mm above the jet exit plane. A reference case at 9% O_2 and 5 atm For the Arrhenius coefficients is also included. The temperature for Arrhenius coefficients is 1300 K.

Radial profiles of temperature in Fig. 13(a, c, e) are well captured when comparing the detailed and single-step mechanisms. The low temperature rise observed in the reaction zone is consistent with experimental observations of both 3% and 9% O_2 JHC flames [27,121]. Whilst the peak temperature of the one-step 9% O_2 case is around 50 K below that of the detailed chemistry at 50 mm, the agreement is still strong, especially across the coflow-jet mixing zone, and in the peak zones. When the pressure in the Arrhenius coefficient function is set to 5 atm, the resulting single-step mechanism shows no ignition at all, highlighting the importance of matching the estimated chemistry to the boundary conditions. Heat release, presented in Fig. 13(b, d, f), does not agree to the same extent as temperature. Over-prediction of heat release rate is prominent at all distances downstream of the jet exit, especially in the 9% O_2 cases. As with the opposed flow diffusion flames, the increase in O_2 at 9%, as well as the lack of decomposition and pyrolysis reactions in the single-step cases result in the significant increase in peak heat release rate, however, a more narrow flame. It is suggested that due to the lack of pyrolysis and radical intermediates, the flame width of the single-step chemistry case is reduced when compared to that of the detailed chemistry. The accuracy of temperature prediction and overall heat release using a single-step mechanism, rather than one with 325 reactions, indicates that the method developed in this work can be used in lieu of a detailed mechanism, at least for initial computations.

3.5. Advantages and limitations of the proposed single-step mechanisms

This work focussed on temperatures above autoignition for the investigated fuels, i.e. above 700 K. The chemistry of methane can become quite complex in these conditions as well, following different pathways to the high temperature combustion conditions [113,114]. Low temperature combustion, whilst relevant to other conventional combustion scenarios, is not the focus of this work. The condition where the initial temperature of the reactants is above autoignition is the prime area of interest.

Increases in temperature to greater than 1500 K, especially at atmospheric conditions, would be likely to result in greater over-prediction of the final temperature, as observed in Fig. 7. However, increases in pressure drive this over-prediction down, implying that there would be good agreement at high pressure and high temperatures, such as in a gas turbine combustion chamber.

The approach proposed could be extended to multi-step combustion, with some modifications to the formulation. In terms of multi-step reactions, the governing equation that was used to derive the Arrhenius coefficients could be considered multiple times, with the relevant progress variable for the intermediate steps and oxidiser conditions being considered. An approach such as this could also be considered for multi-fuel combustion, which by nature would require a single-step reaction at minimum for each fuel.

A single-step mechanism, or indeed even a reduced multi-step reaction would be inappropriate for modelling sooty flames, as the complex mechanisms of soot formation would not be captured. This indicates that extension of the single-step approximation is unlikely to be effective for very long chain hydrocarbons, where soot formation typically becomes more prevalent [122].

In both the opposed flow diffusion flames, and in the CFD simulations presented, a significant reduction in computational time was observed through use of the single-step kinetics, as opposed to the detailed kinetics. In the case of the 1D laminar flames, a five-fold decrease in computational time was observed on average, across ~2000 cases. In the case of CFD however, the single-step kinetics resulted in 10–20 times faster convergence, despite the use of ISAT and TDAC in the detailed chemistry simulations. Without both of these chemistry acceleration factors, convergence was achieved 100 times faster in the single-step case, whilst still maintaining high fidelity in temperature and heat release predictions.

4. Conclusions

The activation energies of equivalent single-step oxidation reactions of hydrogen and methane were determined using a novel approach for a range of environmental conditions. Simulations of detailed chemistry using closed 0D batch reactors were used to estimate global Arrhenius coefficients, subsequently resulting in a functional fit for each coefficient that is valid across a large range of low-oxygen, high-temperature, and elevated pressure conditions. The functions depend on initial temperature, pressure, and the oxidant O_2 mole fraction.

The morphology of the fitting functions was found to be unique to each fuel, and unique between the coefficients. Activation energy and pre-exponential factor fits showed similar shapes and trends when reactant temperature and O_2 mole fraction were varied for both fuels. However, the temperature exponent fit showed significant differences in morphology for hydrogen and methane when oxidant concentration was varied. Both methane and hydrogen showed relatively little change in temperature exponent with variation in initial temperature. Comparatively, whilst hydrogen displayed a proportional change in amplitude for temperature exponent when oxidant concentration was varied, methane displayed a reversal in the pressure relationship. In addition, the trends for activation energy and pre-exponential factor with increasing initial temperature reversed when comparing hydrogen to methane.

Ignition delay and adiabatic temperature predictions were compared between single-step chemistry models and detailed chemistry. Very good agreement was noted for estimation of the ignition delay across a range of conditions. Whilst equilibrium temperature is over-predicted to a small degree in most cases, it is significantly less prominent when initial temperature is lowered. The over-prediction can be attributed to a lack of pyrolysis of the fuels, as well as a lack of intermediates that absorb heat energy in the single-step mechanisms. The single-step approximation was, however, capable of recreating

the NTC behaviour of *n*-heptane, whereby ignition delay reduces with reduced oxidant temperature.

Simulation of opposed flow laminar flames demonstrated that temperature and heat release profiles, along with extinction strain behaviour could be captured using the single step mechanisms to a high degree of accuracy. Use of the single-step mechanisms also reduced the computation time by a factor of five in most cases, significantly reducing the overall wall time for analysing a range of conditions.

Computational fluid dynamics simulations of the single-step and detailed mechanisms at several oxidant conditions indicate that the overall flame features, especially the radial temperature profiles are well captured using single-step chemistry. Wall time for CFD analysis was reduced by a factor of approximately 100 by using the single-step chemistry. Given the use of single-step mechanisms in fundamental DNS studies of combustion, the agreement between temperature and heat release is promising for accurate studies of MILD combustion with detailed turbulence closure.

CRediT authorship contribution statement

Jordan A.C. Kildare: Writing – review & editing, Writing – original draft, Visualization, Validation, Software, Project administration, Methodology, Investigation, Formal analysis, Data curation, Conceptualization. **Michael J. Evans:** Writing – review & editing, Visualization, Validation, Supervision, Methodology, Investigation, Data curation, Conceptualization. **Zhao Tian:** Writing – review & editing, Validation, Supervision, Software, Investigation, Conceptualization. **Paul R. Medwell:** Writing – review & editing, Visualization, Validation, Supervision, Resources, Project administration, Methodology, Investigation, Data curation, Conceptualization.

Declaration of competing interest

The authors declare that they have no known competing financial interests or personal relationships that could have appeared to influence the work reported in this paper.

Data availability

Data will be made available on request.

Acknowledgements

The authors acknowledge the generous support of the University of Adelaide, Australia, the Australian Research Council (ARC), the United States Asian Office for Research and Development (AOARD), the Australian Government Research Training Program Stipend (RTPS), and supercomputing resources provided by Phoenix HPC at the University of Adelaide.

Appendix A. Supplementary data

Supplementary material related to this article can be found online at https://doi.org/10.1016/j.fuel.2023.130589.

References

[1] IEA. World energy outlook 2022. 2022, URL https://www.iea.org/reports/world-energy-outlook-2021.
[2] Kohse-Höinghaus K. Combustion in the future: The importance of chemistry. Proc Combust Inst 2021;38(1):1–56.
[3] de Joannon M, Langella G, Beretta F, Cavaliere A, Noviello C. Mild combustion: Process features and technological constrains. Combust Sci Technol 2000;153(1):33–50.
[4] Cavaliere A, De Joannon M. Mild combustion. Prog Energy Combust Sci 2004;30(4):329–66.
[5] Proud DB, Evans MJ, Chan QN, Medwell PR. Characteristics of turbulent flames in a confined and pressurised jet-in-hot-coflow combustor. J Energy Inst 2022;105:103–13.
[6] Evans M, Medwell P, Tian Z. Modeling lifted jet flames in a heated coflow using an optimized eddy dissipation concept model. Combust Sci Technol 2015;187(7):1093–109.
[7] Medwell PR, Kalt PA, Dally BB. Simultaneous imaging of OH, formaldehyde, and temperature of turbulent nonpremixed jet flames in a heated and diluted coflow. Combust Flame 2007;148(1–2):48–61.
[8] Galbiati MA, Cavigiolo A, Effuggi A, Gelosa D, Rota R. Mild combustion for fuel-NOx reduction. Combust Sci Technol 2004;176(7):1035–54.
[9] Iavarone S, Parente A. NO_x formation in MILD combustion: Potential and limitations of existing approaches in CFD. Front Mech Eng 2020;6:13.
[10] Sabia P, Sorrentino G, Ariemma GB, Manna MV, Ragucci R, de Joannon M. MILD combustion and biofuels: A minireview. Energy Fuels 2021;35(24):19901–19.
[11] Özdemir I, Peters N. Characteristics of the reaction zone in a combustor operating at mild combustion. Exp Fluids 2001;30(6):683–95.
[12] Evans M, Chinnici A, Medwell P, Ye J. Ignition features of methane and ethylene fuel-blends in hot and diluted coflows. Fuel 2017;203:279–89.
[13] Ferrarotti M, Li Z, Parente A. On the role of mixing models in the simulation of MILD combustion using finite-rate chemistry combustion models. Proc Combust Inst 2019;37(4):4531–8.
[14] Dally BB, Karpetis A, Barlow R. Structure of turbulent non-premixed jet flames in a diluted hot coflow. Proc Combust Inst 2002;29(1):1147–54.
[15] Chinnici A, Tian ZF, Lim JH, Nathan GJ, Dally BB. Thermal performance analysis of a syngas-fuelled hybrid solar receiver combustor operated in the MILD combustion regime. Combust Sci Technol 2019;191(1):2–17.
[16] Huang M, Li R, Xu J, Cheng S, Deng H, Zhang B, Rong Z, Li Y. Effect of thermal input, excess air coefficient and combustion mode on natural gas MILD combustion in industrial-scale furnace. Fuel 2021;302:121179.
[17] Evans MJ, Chinnici A. Water vapour effects on temperature and soot loading in ethylene flames in hot and vitiated coflows. Proc Combust Inst 2021;38(4):5383–91.
[18] Liu C, Chen G, Jin Y, Hu X, Lu J. Experimental studies on soot in MILD oxy-coal combustion flame: Sampling, microscopic characteristics, chemical compositions and formation mechanism. Combust Flame 2022;241:112094.
[19] Ye J, Medwell PR, Varea E, Kruse S, Dally BB, Pitsch HG. An experimental study on MILD combustion of prevaporised liquid fuels. Appl Energy 2015;151:93–101.
[20] Proud DB, Evans MJ, Chan QN, Medwell PR. Dilute spray flames of ethanol and n-heptane in the transition to mild combustion. Combust Flame 2022;238:111918.
[21] Saha M, Dally BB, Medwell PR, Chinnici A. Effect of particle size on the MILD combustion characteristics of pulverised brown coal. Fuel Process Technol 2017;155:74–87.
[22] Doan NAK, Swaminathan N. Autoignition and flame propagation in non-premixed MILD combustion. Combust Flame 2019;201:234–43.
[23] Kildare JA, Evans MJ, Proud DB, Chin R, Tian Z, Medwell PR. Characterisation of hydrogen jet flames under different pressures with varying coflow oxygen concentrations. Int J Hydrogen Energy 2023;48(52):20059–76.
[24] Ali G, Zhang T, Wu W, Zhou Y. Effect of hydrogen addition on NOx formation mechanism and pathways in MILD combustion of H2-rich low calorific value fuels. Int J Hydrogen Energy 2020;45(15):9200–10.
[25] Mardani A, Mahalegi HKM. Hydrogen enrichment of methane and syngas for MILD combustion. Int J Hydrogen Energy 2019;44(18):9423–37.
[26] Ye J, Medwell PR, Dally BB, Evans MJ. The transition of ethanol flames from conventional to MILD combustion. Combust Flame 2016;171:173–84.
[27] Medwell PR, Kalt PA, Dally BB. Imaging of diluted turbulent ethylene flames stabilized on a jet in hot coflow (JHC) burner. Combust Flame 2008;152(1–2):100–13.
[28] Ye J, Medwell PR, Evans MJ, Dally BB. Characteristics of turbulent n-heptane jet flames in a hot and diluted coflow. Combust Flame 2017;183:330–42.
[29] Saha M, Dally BB, Medwell PR, Chinnici A. Burning characteristics of victorian brown coal under MILD combustion conditions. Combust Flame 2016;172:252–70.
[30] Vascellari M, Cau G. Influence of turbulence–chemical interaction on CFD pulverized coal MILD combustion modeling. Fuel 2012;101:90–101.
[31] Saha M, Dally BB, Chinnici A, Medwell PR. Effect of co-flow oxygen concentration on the MILD combustion of pulverised coal. Fuel Process Technol 2019;193:7–18.
[32] Abuelnuor A, Wahid M, Hosseini SE, Saat A, Saqr KM, Sait HH, Osman M. Characteristics of biomass in flameless combustion: A review. Renew Sustain Energy Rev 2014;33:363–70.
[33] Hu F, Li P, Cheng P, Liu Y, Shi G, Gao Y, Liu Z. A pilot-scale experimental study on MILD combustion of sawdust and residual char solid waste blend using low-temperature preheating air. Fuel 2023;342:127768.
[34] Weber R, Smart JP, vd Kamp W. On the (MILD) combustion of gaseous, liquid, and solid fuels in high temperature preheated air. Proc Combust Inst 2005;30(2):2623–9.

[35] Wang Z, Feser JS, Lei T, Gupta AK. Performance and emissions of camelina oil derived jet fuel blends under distributed combustion condition. Fuel 2020;271:117685.

[36] Tu Y, Xu M, Zhou D, Wang Q, Yang W, Liu H. CFD and kinetic modelling study of methane MILD combustion in O2/N2, O2/CO2 and O2/H2O atmospheres. Appl Energy 2019;240:1003–13.

[37] Sun L, Xie K, Sun R, Zhang Z, Yan Y, Yuan M, Wu J. Bluff-body MILD combustion regime for semicoke and bituminous coal mixtures with effect of oxidizer O2 concentration in O2/N2 and oxy-fuel (O2/CO2) atmospheres. Fuel 2023;331:125793.

[38] Shaker A, Hashemi SA, Fordoei EE. Numerical study of the O2/CO2, O2/CO2/N2, and O2/N2-syngas MILD combustion: Effects of oxidant temperature, O2 mole fraction, and fuel blends. IN PRESS, 2023,

[39] Evans MJ, Medwell PR, Tian ZF, Ye J, Frassoldati A, Cuoci A. Effects of oxidant stream composition on non-premixed laminar flames with heated and diluted coflows. Combust Flame 2017;178:297–310.

[40] Mi J, Li P, Wang F, Cheong K-P, Wang G. Review on MILD combustion of gaseous fuel: Its definition, ignition, evolution, and emissions. Energy Fuels 2021;35(9):7572–607.

[41] Stefanizzi M, Capurso T, Filomeno G, Torresi M, Pascazio G. Recent combustion strategies in gas turbines for propulsion and power generation toward a zero-emissions future: Fuels, burners, and combustion techniques. Energies 2021;14(20):6694.

[42] Luan C, Xu S, Shi B, Tu Y, Liu H, Li P, Liu Z. Re-recognition of the MILD combustion regime by initial conditions of T in and X O2 for methane in a nonadiabatic well-stirred reactor. Energy Fuels 2020;34(2):2391–404.

[43] Evans M, Medwell P, Wu H, Stagni A, Ihme M. Classification and lift-off height prediction of non-premixed MILD and autoignitive flames. Proc Combust Inst 2017;36(3):4297–304.

[44] de Joannon M, Sabia P, Sorrentino G, Cavaliere A. Numerical study of mild combustion in hot diluted diffusion ignition (HDDI) regime. Proc Combust Inst 2009;32(2):3147–54.

[45] Ye J, Medwell PR, Kleinheinz K, Evans MJ, Dally BB, Pitsch HG. Structural differences of ethanol and DME jet flames in a hot diluted coflow. Combust Flame 2018;192:473–94.

[46] de Joannon M, Sorrentino G, Cavaliere A. MILD combustion in diffusion-controlled regimes of hot diluted fuel. Combust Flame 2012;159(5):1832–9.

[47] Peters N. Laminar flamelet concepts in turbulent combustion, 21 (1) (1988) 1231–1250.

[48] Mauß F, Peters N. Reduced kinetic mechanisms for premixed methane-air flames. In: Reduced kinetic mechanisms for applications in combustion systems. Springer; 1993, p. 58–75.

[49] Oberlack M, Arlitt R, Peters N. On stochastic Damköhler number variations in a homogeneous flow reactor. Combust Theory Model 2000;4(4):495.

[50] Peters N. Turbulent combustion. Cambridge monographs on mechanics, Cambridge: Cambridge University Press; 2000.

[51] Burke S, Schumann T. Diffusion flames. Ind Eng Chem 1928;20(10):998–1004.

[52] Wu W, Mei Y, Zhang L, Liu R, Cai J. Kinetics and reaction chemistry of pyrolysis and combustion of tobacco waste. Fuel 2015;156:71–80.

[53] Parente A, Malik MR, Contino F, Cuoci A, Dally BB. Extension of the Eddy dissipation concept for turbulence/chemistry interactions to MILD combustion. Fuel 2016;163:98–111.

[54] Sabia P, De Joannon M. Critical issues of chemical kinetics in MILD combustion. Front Mech Eng 2020;6:7.

[55] Aminian J, Galletti C, Tognotti L. Extended EDC local extinction model accounting finite-rate chemistry for MILD combustion. Fuel 2016;165:123–33.

[56] Marinov N, Westbrook C, Pitz W. Detailed and global chemical kinetics model for hydrogen. Transp Phenom Combust 1996;1:118.

[57] Bane S, Ziegler J, Shepherd J. Development of one-step chemistry models for flame and ignition simulation. Tech. rep. FM2010-002, Graduate Aeronautical Laboratories, California Institute of Technology; 2010, URL https://shepherd.caltech.edu/EDL/publications/reprints/galcit_fm2010-002.pdf.

[58] Bane S. Spark ignition: Experimental and numerical investigation with application to aviation safety (Ph.D. thesis), California Institute of Technology; 2010.

[59] Bane SP, Ziegler JL, Shepherd JE. Investigation of the effect of electrode geometry on spark ignition. Combust Flame 2015;162(2):462–9.

[60] Carbajal-Carrasco LA, Bouali Z, Mura A. Optimized single-step (OSS) chemistry for auto-ignition of heterogeneous mixtures. Combust Flame 2021;227:11–26.

[61] Le Boursicaud M, Carbajal-Carrasco LA, Bouali Z, Mura A. Optimized two-step (OTS) chemistry model for the description of partially premixed combustion. Combust Flame 2022;245:112287.

[62] Zhang Y, Liu Y. Numerical simulation of hydrogen combustion: global reaction model and validation. Front Energy Res 2017;5:31.

[63] Fernández-Tarrazo E, Sánchez AL, Liñán A, Williams FA. A simple one-step chemistry model for partially premixed hydrocarbon combustion. Combust Flame 2006;147(1–2):32–8.

[64] Fernández-Galisteo D, Sánchez A, Liñán A, Williams F. One-step reduced kinetics for lean hydrogen–air deflagration. Combust Flame 2009;156(5):985–96.

[65] Cailler M, Darabiha N, Veynante D, Fiorina B. Building-up virtual optimized mechanism for flame modeling. Proc Combust Inst 2017;36(1):1251–8.

[66] Cailler M, Darabiha N, Fiorina B. Development of a virtual optimized chemistry method. Application to hydrocarbon/air combustion. Combust Flame 2020;211:281–302.

[67] Coffee TP, Kotlar AJ, Miller MS. The overall reaction concept in premixed, laminar, steady-state flames. I. Stoichiometries. Combust Flame 1983;54(1–3):155–69.

[68] Puri I, Seshadri K. Extinction of diffusion flames burning diluted methane and diluted propane in diluted air. Combust Flame 1986;65(2):137–50.

[69] Peters N, Williams F. The asymptotic structure of stoichiometric methane air flames. Combust Flame 1987;68(2):185–207.

[70] Carpio J, Li B, Fernández-Galisteo D, Sánchez AL, Williams FA. Systematically derived one-step kinetics for hydrogen-air gas-turbine combustion. Combust Flame 2023;250:112633.

[71] Weekes RT, Nomura KK, Sánchez AL, Williams FA. A three-step reduced mechanism for MILD combustion. Combust Sci Technol 2022;1–7.

[72] Liu Y, Han D. Numerical study on explosion limits of ammonia/hydrogen/oxygen mixtures: sensitivity and eigenvalue analysis. Fuel 2021;300:120964.

[73] Fernández-Galisteo D, Weiss A, Sánchez AL, Williams FA. A one-step reduced mechanism for near-limit hydrogen combustion with general stoichiometry. Combust Flame 2019;208:1–4.

[74] Lu T, Law CK. Toward accommodating realistic fuel chemistry in large-scale computations. Progress Energy Combust Sci 2009;35(2):192–215.

[75] Attili A, Lamioni R, Berger L, Kleinheinz K, Lapenna PE, Pitsch H, Creta F. The effect of pressure on the hydrodynamic stability limit of premixed flames. Proc Combust Inst 2021;38(2):1973–81.

[76] Magri L, See Y-C, Tammisola O, Ihme M, Juniper M. Multiple-scale thermoacoustic stability analysis of a coaxial jet combustor. Proc Combust Inst 2017;36(3):3863–71.

[77] Pruefert U, Hunger F, Hasse C. The analysis of chemical time scales in a partial oxidation flame. Combust Flame 2014;161(2):416–26.

[78] Luo Y, Ferraro F, Breicher A, Böttler H, Dreizler A, Geyer D, Hasse C, Scholtissek A. A novel flamelet manifold parametrization approach for lean CH_4–H_2–air flames. Int J Hydrogen Energy 2023;48(1):407–21.

[79] Hu F, Li P, Guo J, Liu Z, Wang L, Mi J, Dally B, Zheng C. Global reaction mechanisms for MILD oxy-combustion of methane. Energy 2018;147:839–57.

[80] Andersen J, Rasmussen CL, Giselsson T, Glarborg P. Global combustion mechanisms for use in CFD modeling under oxy-fuel conditions. Energy Fuels 2009;23(3):1379–89.

[81] Regele JD, Knudsen E, Pitsch H, Blanquart G. A two-equation model for non-unity lewis number differential diffusion in lean premixed laminar flames. Combust Flame 2013;160(2):240–50.

[82] Laidler KJ. The development of the arrhenius equation. J Chem Educ 1984;61(6):494.

[83] Medwell PR, Masri AR, Pham PX, Dally BB, Nathan GJ. Temperature imaging of turbulent dilute spray flames using two-line atomic fluorescence. Exp Fluids 2014;55(11):1840.

[84] Medwell PR, Evans MJ, Chan QN, Katta VR. Laminar flame calculations for analyzing trends in autoignitive jet flames in a hot and vitiated coflow. Energy Fuels 2016;30(10):8680–90.

[85] Doan N, Swaminathan N. Role of radicals on MILD combustion inception. Proc Combust Inst 2019;37(4):4539–46.

[86] Li Z, Evans MJ, Ye J, Medwell PR, Parente A. Numerical and experimental investigation of turbulent n-heptane jet-in-hot-coflow flames. Fuel 2021;283:118748.

[87] Li Z, Chen J-Y, Swaminathan N. A skeletal mechanism for MILD combustion of n-heptane/air mixtures. Combust Sci Technol 2022;1–32.

[88] Minamoto Y, Swaminathan N, Cant SR, Leung T. Morphological and statistical features of reaction zones in MILD and premixed combustion. Combust Flame 2014;161(11):2801–14.

[89] Smith GP, Golden DM, Frenklach M, Moriarty NW, Eiteneer B, Goldenberg M, Bowman CT, Hanson RK, Song S, Jr. WCG, Lissianski VV, Qin Z. GRI-mech 3.0. 2000, URL http://www.me.berkeley.edu/gri_mech/.

[90] Zhou C-W, Li Y, Burke U, Banyon C, Somers KP, Ding S, Khan S, Hargis JW, Sikes T, Mathieu O, et al. An experimental and chemical kinetic modeling study of 1, 3-butadiene combustion: Ignition delay time and laminar flame speed measurements. Combust Flame 2018;197:423–38.

[91] Chemical-kinetic mechanisms for combustion applications. Mechanical and Aerospace Engineering (Combustion Research), University of California at San Diego; 2016, URL https://web.eng.ucsd.edu/mae/groups/combustion/mechanism.html.

[92] Ranzi E, Frassoldati A, Stagni A, Pelucchi M, Cuoci A, Faravelli T. Reduced kinetic schemes of complex reaction systems: fossil and biomass-derived transportation fuels. Int J Chem Kinet 2014;46(9):512–42.

[93] Ranzi E, Cavallotti C, Cuoci A, Frassoldati A, Pelucchi M, Faravelli T. New reaction classes in the kinetic modeling of low temperature oxidation of n-alkanes. Combust Flame 2015;162(5):1679–91.

[94] Bagheri G, Ranzi E, Pelucchi M, Parente A, Frassoldati A, Faravelli T. Comprehensive kinetic study of combustion technologies for low environmental impact: MILD and OXY-fuel combustion of methane. Combust Flame 2020;212:142–55.
[95] He L, Clavin P. Premixed hydrogen-oxygen flames. Part I: Flame structure near the flammability limits. Combust Flame 1993;93(4):391–407.
[96] Mitani T, Williams F. Studies of cellular flames in hydrogen-oxygen-nitrogen mixtures. Combust Flame 1980;39(2):169–90.
[97] Iijima T, Takeno T. Effects of temperature and pressure on burning velocity. Combust Flame 1986;65(1):35–43.
[98] de Joannon M, Sabia P, Tregrossi A, Cavaliere A. Dynamic behavior of methane oxidation in premixed flow reactor. Combust Sci Technol 2004;176(5–6):769–83.
[99] de Joannon M, Cavaliere A, Faravelli T, Ranzi E, Sabia P, Tregrossi A. Analysis of process parameters for steady operations in methane mild combustion technology. Proc Combust Inst 2005;30(2):2605–12.
[100] Sabia P, Sorrentino G, Chinnici A, Cavaliere A, Ragucci R. Dynamic behaviors in methane MILD and oxy-fuel combustion. Chemical effect of CO_2. Energy Fuels 2015;29(3):1978–86.
[101] Dally B, Fletcher D, Masri A. Flow and mixing fields of turbulent bluff-body jets and flames. Combust Theory Model 1998;2(2):193.
[102] Magnussen BF. The eddy dissipation concept: A bridge between science and technology. ECCOMAS Thematic Conf Comput Combust 2005;21:24.
[103] Ertesvåg IS, Magnussen BF. The eddy dissipation turbulence energy cascade model. Combust Sci Technol 2000;159(1):213–35.
[104] Ertesvåg IS. Analysis of some recently proposed modifications to the Eddy dissipation concept (EDC). Combust Sci Technol 2020;192(6):1108–36.
[105] Ertesvåg IS. Scrutinizing proposed extensions to the Eddy dissipation concept (EDC) at low turbulence Reynolds numbers and low Damköhler numbers. Fuel 2022;309:122032.
[106] Péquin A, Evans MJ, Chinnici A, Medwell PR, Parente A. The reactor-based perspective on finite-rate chemistry in turbulent reacting flows: A review from traditional to low-emission combustion. Appl Energy Combust Sci 2023;100201.
[107] Lewandowski MT, Parente A, Pozorski J. Generalised Eddy dissipation concept for MILD combustion regime at low local Reynolds and Damköhler numbers. Part 1: Model framework development. Fuel 2020;278:117743.
[108] Lewandowski MT, Li Z, Parente A, Pozorski J. Generalised Eddy dissipation concept for MILD combustion regime at low local Reynolds and Damköhler numbers. Part 2: Validation of the model. Fuel 2020;278:117773.
[109] Mardani A, Nazari A. Dynamic adjustment of the Eddy dissipation concept model for turbulent/combustion interactions in mixed combustion regimes. Combust Flame 2022;241:111873.
[110] Benson SW, Berson JA. The effect of pressure on the rate and equilibrium constants of chemical reactions. The calculation of activation volumes by application of the tait equation. J Am Chem Soc 1962;84(2):152–8.
[111] Law C. Propagation, structure, and limit phenomena of laminar flames at elevated pressures. Combust Sci Technol 2006;178(1–3):335–60.
[112] Kéromnès A, Metcalfe WK, Heufer KA, Donohoe N, Das AK, Sung C-J, Herzler J, Naumann C, Griebel P, Mathieu O, et al. An experimental and detailed chemical kinetic modeling study of hydrogen and syngas mixture oxidation at elevated pressures. Combust Flame 2013;160(6):995–1011.
[113] Sabia P, de Joannon M, Picarelli A, Chinnici A, Ragucci R. Modeling negative temperature coefficient region in methane oxidation. Fuel 2012;91(1):238–45.
[114] Sabia P, de Joannon M, Picarelli A, Ragucci R. Methane auto-ignition delay times and oxidation regimes in MILD combustion at atmospheric pressure. Combust Flame 2013;160(1):47–55.
[115] de Joannon M, Saponaro A, Cavaliere A. Zero-dimensional analysis of diluted oxidation of methane in rich conditions. Proc Combust Inst 2000;28(2):1639–46.
[116] Burke U, Somers KP, O'Toole P, Zinner CM, Marquet N, Bourque G, Petersen EL, Metcalfe WK, Serinyel Z, Curran HJ. An ignition delay and kinetic modeling study of methane, dimethyl ether, and their mixtures at high pressures. Combust Flame 2015;162(2):315–30.
[117] Krisman A, Hawkes ER, Chen JH. The structure and propagation of laminar flames under autoignitive conditions. Combust Flame 2018;188:399–411.
[118] Ciezki H, Adomeit G. Shock-tube investigation of self-ignition of n-heptane-air mixtures under engine relevant conditions. Combust Flame 1993;93(4):421–33.
[119] Curran HJ, Gaffuri P, Pitz WJ, Westbrook CK. A comprehensive modeling study of n-heptane oxidation. Combust Flame 1998;114(1–2):149–77.
[120] Zhang K, Banyon C, Bugler J, Curran HJ, Rodriguez A, Herbinet O, Battin-Leclerc F, B'Chir C, Heufer KA. An updated experimental and kinetic modeling study of n-heptane oxidation. Combust Flame 2016;172:116–35.
[121] Christo FC, Dally BB. Modeling turbulent reacting jets issuing into a hot and diluted coflow. Combust Flame 2005;142(1–2):117–29.
[122] Kent J. A quantitative relationship between soot yield and smoke point measurements. Combust Flame 1986;63(3):349–58.